Influence of the material anisotropy in the estimation of the yield strength with the Small Punch Test

Jose Calaf-Chica[(1)], Pedro Miguel Bravo Díez[(2)], Mónica Preciado Calzada[(3)]

E-mails: (1) Corresponding author, jcalaf@ubu.es ; (2) pmbravo@ubu.es; (3) mpreciado@ubu.es
Postal address: Departamento de Ingeniería Civil, Universidad de Burgos, Avenida Cantabria s/n, E09006 Burgos, Spain

ABSTRACT

The Small Punch Test (SPT) was developed in the 80's as an alternative miniature test for the characterization of mechanical properties in the nuclear industry. One of the key aspects that materials must fulfill to be used with this miniature test is that of homogeneity and isotropy. The origin of the isotropy requirement comes from the fact that the estimation of mechanical properties using the SPT requires empirical correlations with standard tests, which generally show uniaxial stress fields. By contrast, the SPT shows a multiaxial stress field. There are few publications related with the influence of material anisotropy in the yield strength estimation using the SPT, and most of them are empirical studies. This research was intended to address, with a systematic finite element analysis, the influence that different anisotropy combinations could show in the yield strength estimation using the SPT. Thirty-six anisotropic hypothetical materials were evaluated with SPT simulations using the Hill'48 yield criterion. The yield strength of each material was estimated with the SPT using four correlation methods: Mao's, CEN's, the t/10 offset, and the optimized t/10. This study concluded that the SPT was not an appropriate test to evaluate or quantify the material anisotropy, but it was a valuable experimental test to estimate a mean yield strength of the six yielding stress components of the anisotropic material.

Keywords: Small Punch Test, SPT, yield strength, anisotropy.

Note: This research did not receive any specific grant from funding agencies in the public, commercial, or non-profit sectors.

1 Introduction

The miniature tests for the characterization of mechanical properties of metallic materials were developed in the nuclear sector in the 80's supported by different research programs [1,2]. The new generations of the nuclear plants and the design concept development of a novel nuclear fusion plant made it necessary to characterize the embrittlement process in the different structural components in the nuclear reactor.

The standard tests for the estimation of mechanical properties showed a specimen volume which greatly limited the number of specimens that could be introduced in the nuclear reactor. In addition, higher volume implied an exponential increment in the required irradiation times [3,4]. This limitation was the main motivation for the development of the Small Punch Test (SPT) in 1981 [5]. From that period on, there have been two trends in the research focused on this miniature test: firstly, investigations that progressed in the understanding of the test and in increasing its reliability and secondly, research that extended or adapted the test for the characterization of new mechanical properties. The research focusing on this second point was carried out by means of the SPT for the estimation of a variety of mechanical properties: Young's modulus [6], yield strength [7,8], ultimate tensile strength [9,10], ductile-to-brittle transition temperature [11,12], fracture toughness [13,14], creep [15,16], fatigue life [17], etc. In 2006, CEN Workshop Agreement CWA 15627 was published to provide a guidance of the experimental conditions in the SPT [18]. The standard prEN 10371, related with the use of the SPT in metallic materials, is expected to be published soon [19].

All these applications had a key aspect of the SPT in common: the mechanical properties were not obtained directly but rather were estimated with different empirical correlation equations that related the obtained data from the SPT to each specific mechanical property obtained from a standard test for the same material. The complex tensile and deformation fields which are generated during this miniature test hindered the development of a reliable analytical-theoretical models, which were saved by the use of empirical correlation equations.

Figure 1(a) shows a schematic view of the SPT set-up and the basic nomenclature of the different SPT tools. It is made up of two dies, lower and upper, that clamp down on the specimen and a spherical punch that indents the specimen until failure. The geometrical parameters of the different parts are: a lower die, with an internal hole of R_d = 4 mm and a filled radius of r = 0.5 mm; an upper die, with an internal hole of R_p = 1.25 mm to guide the punch displacement; a spherical punch with a diameter of 2.5 mm; a specimen or disk with a thickness t = 0.5±0.005 mm and a diameter equal to d = 8 mm. During the test, the punch load and the punch displacement are registered to generate the load-displacement curve, generally called the SPT curve, shown in Figure 1(b).

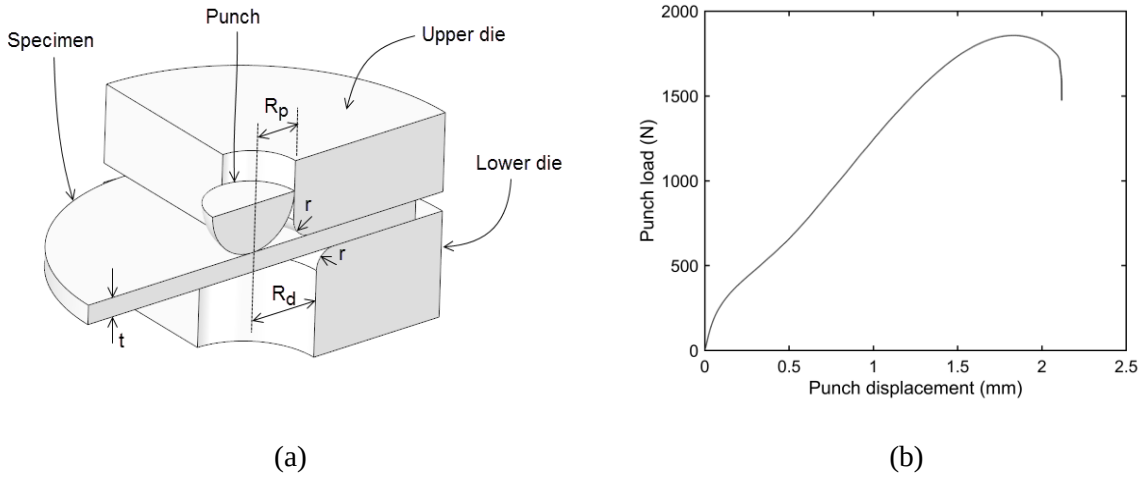

(a) (b)

Figure 1. (a) SPT set-up and (b) experimental SPT curve

For the specific case of mechanical properties inherent to the uniaxial tensile test, one of the most essential requirements of the evaluated material in an SPT specimen is its isotropy. This necessity is based on the fact that the standard tensile test generates a uniaxial stress field, and it evaluates the mechanical properties in only one specific direction. By contrast, the SPT generates multiaxial stress and strain fields, where mechanical properties in every direction come into play (axial and shear). Thus, in the case of the evaluation of anisotropic materials, the estimated mechanical property with the SPT could show significant deviations in a comparison with the value obtained in a uniaxial tensile test.

One of the first publications which dealt with the influence of anisotropy in the reliability of the SPT was the investigation of Campitelli et al. [20]. They estimated the yield strength anisotropy of Zircaloy tubes with tensile tests and studied its influence in SPT correlations for the same material. With the aim of strengthening this empirical study, a finite element (FEM) analysis was performed using the Hill'48 yield criterion [21] in order to include the anisotropic behavior of Zircaloy. Due to the geometrical limitations of the analyzed tubes, they could not empirically estimate the 6 constants of the Hill yield criterion. Through FEM simulations, different values for the unknown constants of the Hill yield criterion were evaluated until enough agreement was reached between the experimental and numerical SPT curves. It is worth noting that the authors verified that a similar response could be obtained in the SPT simulations with more than one combination of the Hill yield criterion constants. In conclusion, the SPT was not a robust test for the quantification of the yield strength anisotropy.

Okuda et al. [22] empirically evaluated the influence of anisotropy in the ductile-to-brittle transition temperature estimated using the SPT for an ODS ferritic steel. Wha et al. [23] detected that the presence of anisotropy in the 2024 aluminum alloy affected the estimation of the yield strength and the ultimate tensile strength with the SPT. Turba et al. [24] deduced that the anisotropy in ODS ferritic steels modified the creep rupture times and ductile-to-brittle

transitions temperatures of the SPT specimens according to the orientation from which they were extracted (longitudinal or transversal). These differences were related to the strong elongated grains of the microstructure. These grains could be oriented on the plane of the SPT specimen (longitudinal) or normally to the specimen (transversal). The latter of the two made the initiation of cracks and damage for a lower plastic strain easier. The different behavior of the SPT specimens depending on the extraction position has been extensively studied for different materials (pure titanium [25] or ODS steels [26,27,28]). Song et al. [29] analyzed the anisotropic behavior of an A350 alloy forged flange with tensile and SPT tests. The yield strength and ultimate tensile strength estimations with the SPT were well-matched with the results obtained with the standard tensile tests only when the normal direction of the SPT specimen was parallel to the axis of the tensile specimen. Similar empirical investigations have been published for other materials like Zr-2.5% Nb alloy [30] or Inconel 718 [31].

The aim of this investigation was to study the conduct of an FEM simulation survey to evaluate how anisotropy influenced the SPT and its estimation reliability of the yield strength.

2 Materials and Methods

There is a wide range of estimation methodologies for the yield strength using the SPT. This investigation focused on four of them: Mao's or the two tangent method [2], CEN's method [32], the t/10 offset method [33], and the optimized t/10 offset method [34]. Figure 2 shows the different parameters that are extracted from the SPT curve for each methodology: Mao's method, which uses the yield load P_y obtained from the cross point of two tangents at the initial maximum slope and the minimum slope of the SPT curve; CEN's method, which uses the yield load P_y derived from a bilinear equation that minimizes error with the SPT curve; the t/10 offset method, where the yield load P_y is obtained with the cross point of the SPT curve and a parallel offset line to the initial maximum slope (offset equal to a tenth of the specimen thickness: 0.5/10 = 0.05 mm); the optimized t/10 offset method, which uses the yield load P_y obtained in the t/10 offset method and the minimum slope $Slope_{min}$. The correlation equations (1) for Mao's, CEN's, and t/10 offset methods, and (2) for the optimized t/10 offset method, relate these parameters of the SPT curve to the yield strength. The constants or correlation coefficients α_1, α_2, β_1 y β_2 must be calculated empirically. This investigation used these four correlation methods for the evaluation of the obtained SPT curves.

$$\sigma_y = \alpha_1 \frac{P_y}{t^2} + \alpha_2 \tag{1}$$

$$\sigma_y = \beta_1 \frac{P_y}{t^2} + \beta_2 \frac{Slope_{min}}{t} \tag{2}$$

where:
α_1, α_2, β_1 and β_2 are correlation coefficients obtained in the empirical linear regression,
and t is the specimen thickness.

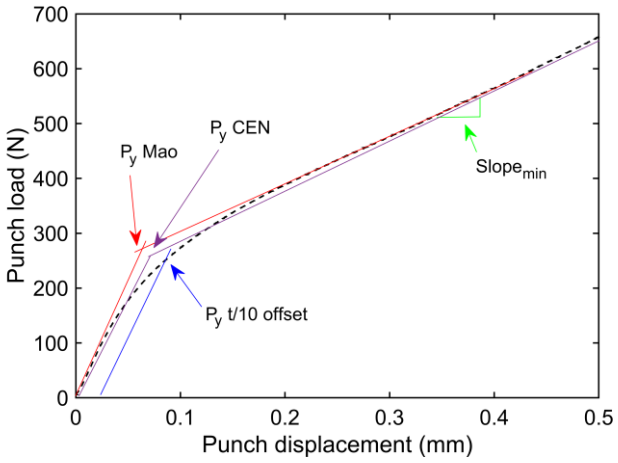

Figure 2. Parameters used in the correlation methods for the yield strength estimation using the SPT

A group of 36 hypothetical materials were designed to perform the FEM simulations. All of them had the mechanical properties included in Table 1 in common. The simulation of the strain hardening was performed using the Ramberg-Osgood hardening law and following the equation (3).

E (GPa)	ν	σ_y (MPa)	n
200	0.3	400	10

Table 1. Mechanical properties of the hypothetical materials

$$\varepsilon_{true} = \frac{\sigma_{true}}{E} + \varepsilon_{offset}\left(\frac{\sigma_{true}}{\sigma_y}\right)^n \quad (3)$$

where:
$\varepsilon_{offset} = 0.002$ is the plastic strain of the offset yield point
σ_{true} is the true stress
ε_{true} is the true strain
E is Young's modulus
σ_y is the yield strength
and n is the hardening coefficient

In order to simulate the presence of anisotropy in these hypothetical materials, the FEM model implemented the Hill'48 yield criterion [21]. Equation (4) shows the yield surface of the Hill'48 model. The parameters F, G, H, L, M and N define the anisotropy level of each stress field component. For the specific case with $F = G = H = 1/2$ and $L = M = N = 3/2$, the Hill model is equivalent to the isotropic Von Mises yield criterion.

$$\sigma_y^2 = F(\sigma_{22} - \sigma_{33})^2 + G(\sigma_{33} - \sigma_{11})^2 + H(\sigma_{11} - \sigma_{22})^2 + 2L\sigma_{23}^2 + 2M\sigma_{31}^2 + 2N\sigma_{12}^2 \quad (4)$$

These simulations were performed with ANSYS v18.2 software, where the Hill'48 model is characterized with 6 R_{ij} factors which relate each yielding stress component (σ_{ij}^y) with the isotropic yield strength introduced in the hardening model (σ_y = 400 MPa, as shown in Table 1). Equations (5) and (6) show the R factors formulation and its relation with the coefficients of the Hill'48 model.

$$\boldsymbol{R_{ij}} = \frac{\boldsymbol{\sigma_{ij}^y}}{\boldsymbol{\sigma_y}} \quad (5)$$

$$F = \frac{1}{2}\left(\frac{1}{R_{22}^2} + \frac{1}{R_{33}^2} - \frac{1}{R_{11}^2}\right) \qquad L = \frac{1}{2}\left(\frac{1}{R_{23}^2}\right)$$
$$G = \frac{1}{2}\left(\frac{1}{R_{33}^2} + \frac{1}{R_{11}^2} - \frac{1}{R_{22}^2}\right) \qquad M = \frac{1}{2}\left(\frac{1}{R_{13}^2}\right) \quad (6)$$
$$H = \frac{1}{2}\left(\frac{1}{R_{11}^2} + \frac{1}{R_{22}^2} - \frac{1}{R_{33}^2}\right) \qquad \boldsymbol{N = \frac{1}{2}\left(\frac{1}{R_{12}^2}\right)}$$

The simulations considered two alternative values for the R factors of the hypothetical materials: R = 0.7 and R = 1.0. In the case of R = 1.0, the yielding stress component was equal to the yield strength of the isotropic hardening model

introduced in the analysis (σ_y = 400 MPa). When R = 0.7, the yielding stress component was equal to $\sigma_{ij}^{y} = 0.7 \cdot \sigma_y$ = 280 MPa.

The SPT tools (punch and upper and lower dies) were established in the simulations as rigid bodies, fixing the dies position and controlling the vertical displacement of the spherical punch. The contacts between the different parts had a friction coefficient of 0.1. Considering that the anisotropy was established using the global coordinate system of the simulation, the simplification of the SPT to an axisymmetric model was dismissed, and a 3D geometry was designed making the most of the model symmetries. The xz plane corresponded to the SPT specimen plane, and the y axis corresponded to the punch displacement direction. Figure 3(b) shows the 3D FEM model. Based on SPT simulations with axisymmetric models and experimentally validated in previous research [35], the 3D FEM model was validated by means of a comparison with an equivalent axisymmetric model, seen Figure 3(a). To this end, the axisymmetric model used a material model based on the mechanical properties included in Table 1 with the Von Mises yield criterion. The 3D FEM model used the same mechanical properties but using the Hill'48 yield criterion with all the coefficients R = 1.0 (equivalent to a Von Mises model). Figure 4 shows the resulting SPT curves where both were well-matched, validating the 3D FEM model.

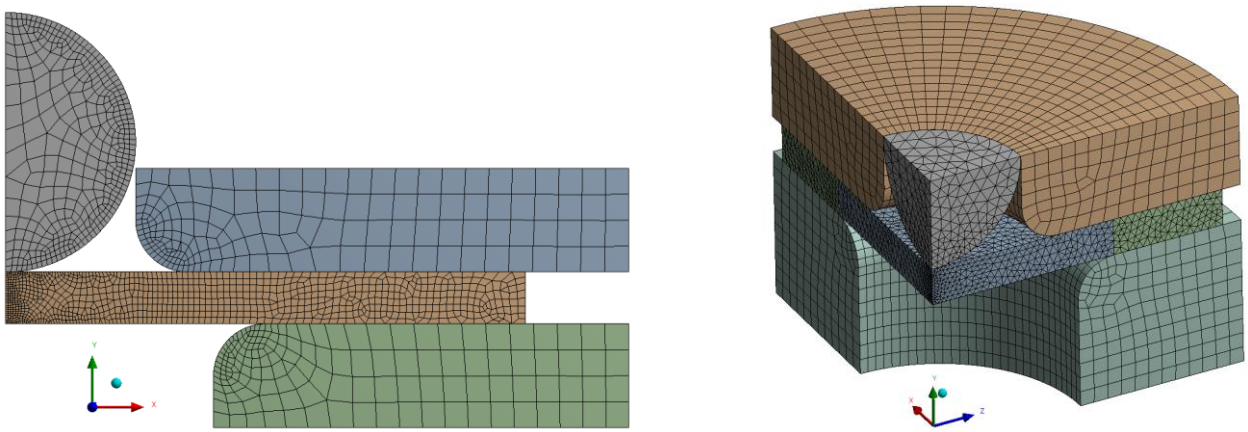

(a) (b)

Figure 3. FEM model of the SPT: (a) axisymmetric model and (b) 3D model

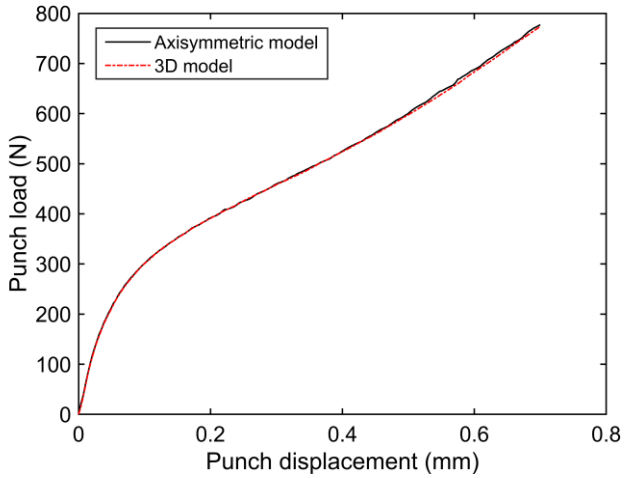

Figure 4. Comparison of the SPT curves for axisymmetric and 3D models

As commented previously, the Hill'48 yield criterion is established with six R factors, and those coefficients had two different values in the simulations of this investigation: 0.7 and 1.0. Combining all the anisotropy possibilities with these two values, there were 2^6 = 64 anisotropic models. But it should be considered that the yielding stress components σ_{xx}^{y} and σ_{zz}^{y} as well as σ_{xy}^{y} and σ_{yz}^{y} show similar behavior due to the model symmetry (see Figure 3(b) to identify the global coordinate system of the 3D model). This means, for example, that the model (R_{xx}, R_{yy}, R_{zz}, R_{xy}, R_{yz}, R_{zx}) = (1.0,

1.0, 0.7, 1.0, 1.0, 1.0) would be equivalent to the model (0.7, 1.0, 1.0, 1.0, 1.0, 1.0). These considerations reduced the anisotropic models to 36 cases, where two of them were equivalent to isotropic Von Mises models: case (1.0, 1.0, 1.0, 1.0, 1.0, 1.0) and case (0.7, 0.7, 0.7, 0.7, 0.7, 0.7). Each anisotropic material was identified with the ID xxxxxx, where *x* could show the values 0, for the case R = 0.7, and 1, for the case R = 1.0. The first three positions of the ID corresponded with the R factors of axial stresses *x*, *y* and *z*, and the last three positions with the R factors of shear stresses *xy*, *yz* and *xz*.

The correlation coefficients should be obtained for each methodology in order to apply the correlation methods for the estimation of the yield strength. To that end, an axisymmetric model of the SPT was simulated with four isotropic hypothetical materials with yield strengths and hardening coefficients *n* around the values established in Table 1. Table 2 shows the mechanical properties used for these simulations and the yield loads P_y and minimum slopes $Slope_{min}$ obtained from their simulated SPT curves. Table 3 shows the correlation coefficients calculated for these four isotropic materials, as well as the coefficients of determination R^2 for each regression. After that, the yield loads P_y and minimum slopes $Slope_{min}$ of the 36 anisotropic hypothetical materials were obtained and the yield strength of each material was estimated using the correlation equations previously calculated with the isotropic materials.

Material	***σ_y* (MPa)**	***n***	***P_y Mao (N)***	***P_y CEN (N)***	***P_y t/10 offset (N)***	***$Slope_{min}$ (N/mm)***
1	200	5	170.0	167.6	187.5	503.3
2	200	30	143.2	144.2	142.0	223.4
3	600	5	477.2	490.7	534.0	1525.1
4	600	30	423.3	395.2	410.0	694.9

Table 2. Mechanical properties and SPT parameters of the isotropic hypothetical materials

	α_1	***α_2***	***β_1***	***β_2***	***R^2***
Mao	0.334	-4.839	-	-	0.979
CEN	0.329	5.908	-	-	0.945
t/10 offset	0.298	20.577	-	-	0.915
Opt. t/10 offset	-	-	0.485	-0.145	0.997

Table 3. Correlation coefficients for the isotropic hypothetical materials

3 Results and discussion

Figure 5 shows the SPT curves of the 36 hypothetical materials. Case ID 000000, which was equivalent to the Von Mises yield criterion with a yield strength of 280 MPa, and ID 111111, which was similar to a Von Mises yield criterion with a yield strength of 400 MPa, have been highlighted in red. These two cases represented the isotropic ends of the 34 anisotropic intermediate cases. The grey curves represent the cases with Hill'48 yield criterion and with a combination of R's 0.7 and 1.0. Most of the anisotropic cases were contained among both isotropic cases. Table 4 shows the yield loads P_y, the minimum slope $Slope_{min}$ and the estimated yield strengths for each methodology using the correlation coefficients included in Table 3.

ID	***P_y Mao (N)***	***P_y CEN (N)***	***P_y t/10 offset (N)***	***$Slope_{min}$ (N/mm)***	***σ_y Mao (MPa)***	***σ_y CEN (MPa)***	***σ_y t/10 offset (MPa)***	***σ_y opt. t/10 offset (MPa)***
111111	305.1	300.6	305.2	624.0	402.8	401.5	384.4	411.1
011111	299.2	296.7	305.5	680.1	394.9	396.3	384.7	395.4
101111	285.6	286.6	286.0	453.5	376.7	383.1	361.5	423.3
010111	278.2	266.2	280.5	590.2	366.9	356.2	354.9	373.0
001111	277.4	258.1	273.0	410.4	365.7	345.6	346.0	410.6
000111	244.1	244.7	252.0	407.2	321.2	327.9	321.0	370.8
111011	290.2	271.8	278.0	632.9	382.8	363.6	352.0	355.8
111110	283.9	270.7	283.5	588.4	374.4	362.2	358.5	379.3
111001	259.1	268.7	265.3	702.0	341.4	359.5	336.8	311.1
111010	270.1	266.4	274.0	621.9	356.0	356.5	347.2	351.2

111000	245.4	242.8	247.5	663.3	323.0	325.4	315.6	287.8
011110	276.1	262.3	282.0	658.9	364.1	351.1	356.7	356.0
011011	289.0	274.7	286.0	702.8	381.2	367.5	361.5	351.0
011010	268.2	220.5	270.0	678.9	353.4	296.0	342.4	326.9
011001	257.0	245.6	255.0	735.4	338.5	329.2	324.5	281.4
101001	264.3	260.7	254.0	502.2	348.3	349.0	323.3	347.1
101110	268.7	274.4	268.0	416.0	354.1	367.0	340.0	399.3
101011	293.4	262.7	269.0	426.3	387.1	351.6	341.2	398.2
101010	260.3	255.6	252.0	424.0	343.0	342.3	321.0	365.9
010001	240.5	241.5	243.0	665.8	316.5	323.7	310.2	278.3
010110	251.0	251.6	258.0	575.4	330.5	336.9	328.1	333.7
010011	270.0	264.4	271.7	609.6	355.9	353.9	344.4	350.2
010010	241.8	234.4	252.7	603.9	318.2	314.3	321.9	315.2
001001	242.5	234.0	239.0	503.0	319.1	313.8	305.5	317.8
001110	252.0	242.7	250.0	389.9	331.8	325.3	318.6	371.9
001011	260.4	259.2	256.4	458.4	343.1	347.1	326.2	364.4
001010	238.9	228.3	237.0	417.4	314.3	306.3	303.1	338.7
000001	236.5	230.2	226.5	416.3	311.2	308.8	290.6	318.7
000110	224.4	219.3	231.0	361.7	294.9	294.5	295.9	343.2
000011	238.6	230.8	238.0	415.0	313.9	309.6	304.3	341.4
000010	217.8	219.5	217.0	378.1	286.2	294.8	279.2	311.3
011000	242.2	242.6	241.0	702.3	318.7	325.2	307.8	263.9
101000	252.7	232.1	238.0	448.0	332.8	311.3	304.3	331.8
010000	224.4	219.4	230.6	630.3	294.9	294.7	295.4	264.5
001000	234.2	228.8	222.5	436.8	308.1	307.0	285.8	305.0
000000	209.0	203.7	210.0	417.0	274.4	273.9	270.9	286.5

Table 4. SPT parameters and estimated yield strengths for the hypothetical materials

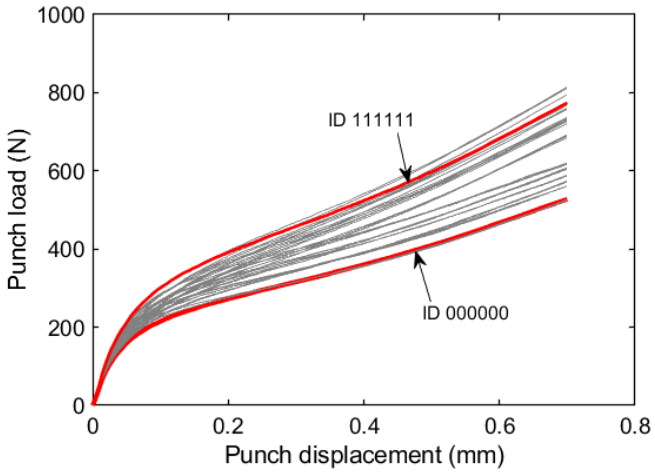

Figure 5. SPT curves for the hypothetical materials

The estimated yield strengths of each correlation method for each hypothetical material changed around the range between 280 MPa and 400 MPa. Thus, the presence of anisotropy, to a greater or lesser extent, generated an intermediate estimation of the yield strength between the isotropic cases ID 000000 (yield strength of 280 MPa), and ID 111111 (yield strength of 400 MPa). Consequently, some critical cases were detected, like ID 010000. This case had anisotropy in the y axis, and as a result, it could show a yield strength of 400 MPa in an uniaxial tensile test aligned with the mentioned y axis, while a SPT specimen perpendicular to the y axis would estimate a yield strength lower than 300 MPa for all the correlation methods used in this investigation (see Table 4). This highlights the significance of avoiding the use of anisotropic materials to obtain correlation coefficients of any method for the estimation of the

yield strength with the SPT, because they could introduce significant biasing depending on the selected axis for the tensile specimen extraction.

After this first analysis of the simulations, the influence of each yielding stress component anisotropy on the estimated yield strength with each correlation method could be discerned. Figure 6 shows the estimated yield strengths with each correlation method for a selection of the 36 hypothetical materials. Cases 011111 and 101111 represented axial anisotropies in the x axis and y axis respectively. Anisotropy in the z axis (case 001111) was not considered because it had the same behavior as ID 011111 due to the inherent symmetries of the SPT. Figure 6 shows that axial anisotropies in x and z axes (that is to say, on the plane of the SPT specimen) did not generate significant changes in the estimation of the yield strength. By contrast, an anisotropy in the y axis (along the specimen thickness) diminished the estimated yield strength in three correlation methods, except the optimized t/10 offset method which showed an increment in the yield strength estimation.

When the anisotropy was applied axially and simultaneously in more than one direction, there were three options: ID 010111, which showed reduced yielding stress in the specimen plane (x and z axes); ID 001111, where the anisotropy was contained in one direction of the specimen plane and the normal axis of the SPT disk (x and y axes); and ID 000111, which diminished the yielding stress of all the three axial directions. In the first case, ID 010111, the results of the four correlation methods were similar with a reduction in the estimated yield strength, with values in the range of the case of a single anisotropy in the y axis. In the case ID 001111, the behavior was slightly lower than cases 010111 and 101111 showed, but with the particularity of the optimized t/10 offset method that, as shown in the case ID 101111, it did not result in any significant alteration of the yield strength estimation for this combination of anisotropies. Finally, ID 000111 was the case that showed the largest drop in the yield strength estimation for anisotropies in the axial directions, but it was still a long way from the isotropic model with a yield strength of 280 MPa. Once again, for this case, the optimized t/10 offset method showed a lower drop than the rest of the correlation methods. In conclusion, a lower yielding stress component in the thickness direction of the SPT specimen (y axis) generated a particularity that stood out in the optimized t/10 offset method: instead of reducing the estimated yield strength, it clearly grew. The results for the rest of the correlation methods showed that the reduction of the yielding stress components contained in the specimen plane (x and z axes) had a lower capacity to influence in the reduction of the yield strength estimation compared to the case with anisotropy in the specimen thickness (y axis).

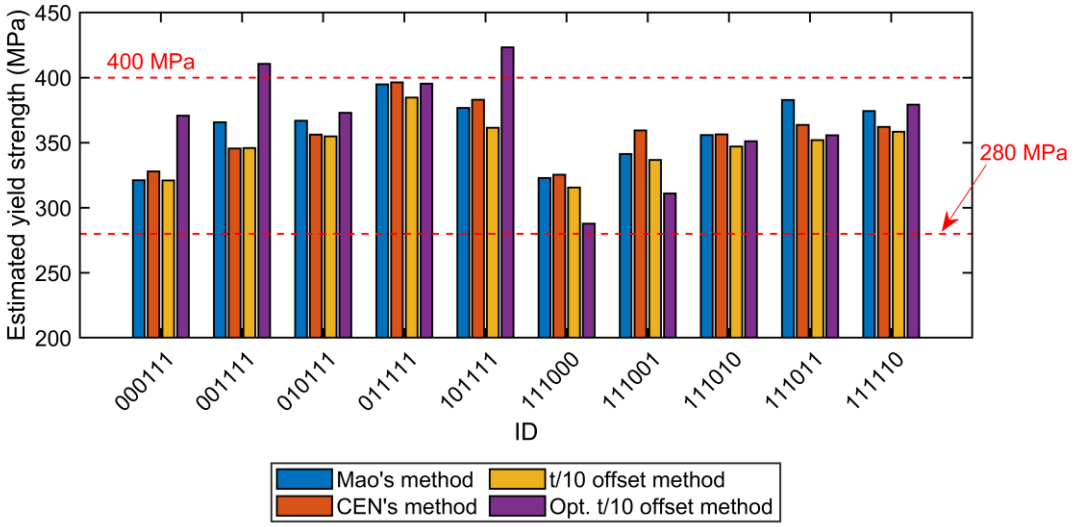

Figure 6. Yield strength estimation for each correlation method

For the cases with anisotropies in the yielding stress components related with shear stresses, all of them showed a higher capability of influence than those reflected by axial anisotropies. In these cases, the optimized t/10 offset method showed more sensitivity compared to the rest of the correlation methods, so much so that case ID 111000 estimated a yield strength very close to isotropic case ID 000000. Thus, all the correlation methods were more sensitive to shear anisotropies than axial ones, with the optimized t/10 method being the one that showed this behavior most clearly.

This numerical study showed the inability of the SPT as an experimental test to estimate anisotropic behavior, because there were different anisotropy scenarios that showed similar yield strength estimations. Cases ID 010111 and 111010, included in Figure 6, are examples of this fact. Nevertheless, this does not mean that the SPT is not an option for anisotropic materials. Figure 7 shows the estimated yield strengths for each correlation method versus the percentage of the yielding stress components with R = 1.0 (identified with the acronym *PYTC*; see equation (7)). A *PYTC* = 100 % matched with an isotropic material with all the yielding stress components with R = 1.0, and *PYTC* = 0 % matched with an isotropic material with all the yielding stress components with R = 0.7. Figure 7 shows that the tendency of the yield strength estimation was to grow linearly with an increment in the *PYTC*. Thus, the SPT worked fine as a test to estimate a mean value of the yielding stress components in anisotropic materials. Of the four correlation methods, the best suited for a linear correlation with the *PYTC* was the t/10 offset method. The optimized t/10 offset method showed the worst deviation values. This is because, as shown in Figure 6, the unequal sensitivity that this method showed for axial anisotropies (low sensitivity) and shear anisotropies (high sensitivites).

$$PYTC = \frac{\text{number of yielding stress components with } R = 1.0}{6} \times 100 \qquad (7)$$

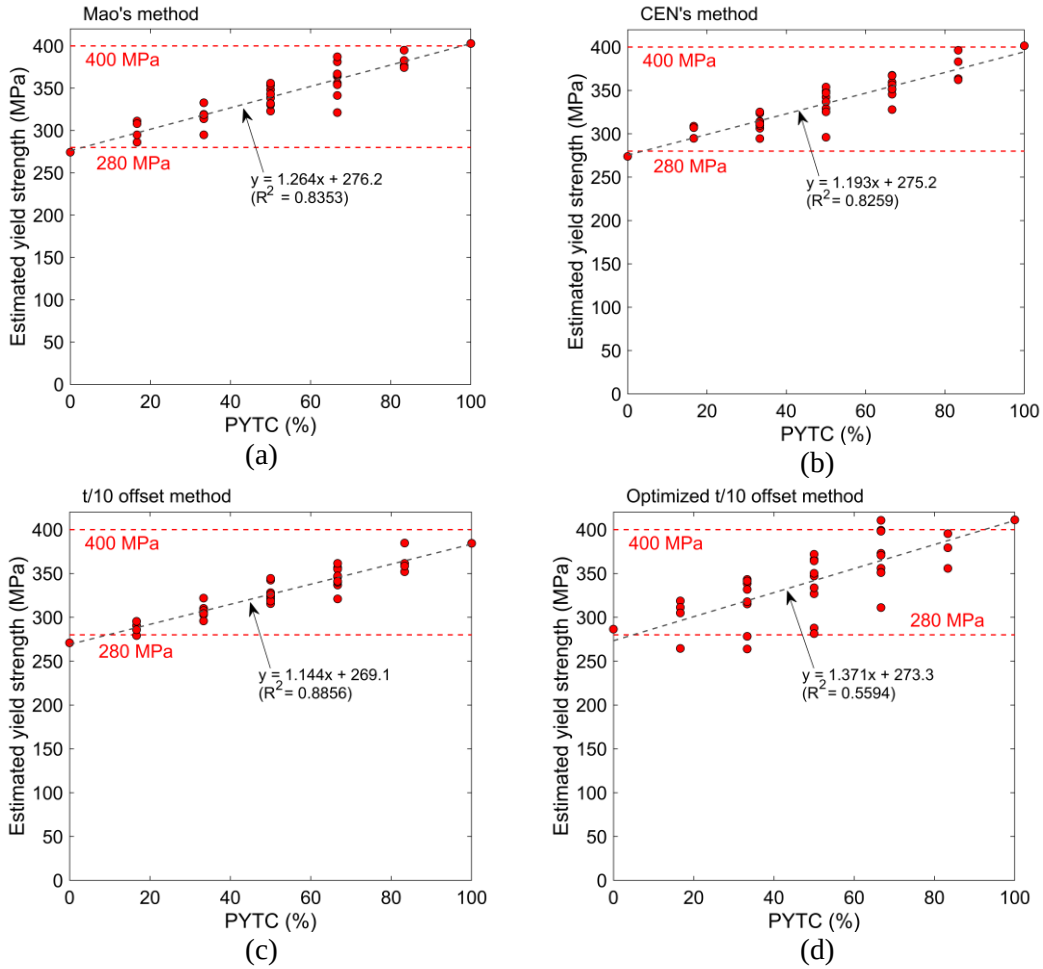

Figure 7. Yield strength estimation versus PYTC: (a) Mao's method, (b) CEN's method, (c) t/10 offset method, and (d) optimized t/10 offset method

4 Conclusions

This investigation, based on a numerical analysis, has drawn the following conclusions:

(a) Materials with anisotropy in some yielding stress components showed an estimated yield strength with the SPT contained between the values of the mentioned yielding stress components.
(b) Anisotropic materials should not be used to obtain the correlation coefficients of the estimation methodologies of the yield strength with the SPT.
(c) Axial anisotropies in the SPT specimen plane did not show significant changes in the estimation of the yield strength, being more sensitive to shear anisotropies.
(d) The SPT was not an appropriate test for anisotropy estimation or quantification, because different combinations of anisotropy generated similar yield strength estimations.
(e) The use of the SPT for anisotropic materials estimated a mean value of the yielding stress components in Mao's, CEN's and t/10 offset correlation methods.

5 Data availability

The raw/processed data required to reproduce these findings cannot be shared at this time as the data also forms part of an ongoing study.

6 References

[1] Baik, Jai Man, J. Kameda, and O. Buck. 1983. "Small Punch Test Evaluation of Intergranular Embrittlement of an Alloy Steel." *Scripta Metallurgica* 17(12):1443–47. DOI: 10.1016/0036-9748(83)90373-3.

[2] Mao, Xinyuan, and Hideaki Takahashi. 1987. "Development of a Further-Miniaturized Specimen of 3 Mm Diameter for Tem Disk (ø 3 Mm) Small Punch Tests." *Journal of Nuclear Materials* 150(1):42–52. DOI: 10.1016/0022-3115(87)90092-4.

[3] Misawa, T., H. Sugawara, R. Miura, and Y. Hamaguchi. 1985. "Small Specimen Fracture Toughness Tests of HT-9 Steel Irradiated with Protons." *Journal of Nuclear Materials* 133–134(C):313–16. DOI: 10.1016/0022-3115(85)90158-8.

[4] Wang, Zhao Xi, Hui Ji Shi, Jian Lu, Pan Shi, and Xian Feng Ma. 2008. "Small Punch Testing for Assessing the Fracture Properties of the Reactor Vessel Steel with Different Thicknesses." *Nuclear Engineering and Design* 238(12):3186–93. DOI: 10.1016/j.nucengdes.2008.07.013.

[5] Manahan, M. P., A. S. Argon, and O. K. Harling. 1981. "The Development of a Miniaturized Disk Bend Test for the Determination of Postirradiation Mechanical Properties." *Journal of Nuclear Materials* 104(C):1545–50. DOI: 10.1016/0022-3115(82)90820-0.

[6] Calaf Chica, José, Pedro Miguel Bravo Díez, and Mónica Preciado Calzada. 2017. "Improved Correlation for Elastic Modulus Prediction of Metallic Materials in the Small Punch Test." *International Journal of Mechanical Sciences* 134C:112–22. DOI: 10.1016/j.ijmecsci.2017.10.006.

[7] Eskner, Mats, and Rolf Sandström. 2004. "Mechanical Property Evaluation Using the Small Punch Test." *Journal of Testing and Evaluation* 32(4):282–89. DOI: 10.1520/jte11504.

[8] Isselin, Jerome, and Tetsuo Shoji. 2009. "Yield Strength Evaluation by Small-Punch Test." *Journal of Testing and Evaluation* 37(6):531–37. DOI: 10.1520/jte101657.

[9] Bruchhausen, M., S. Holmström, I. Simonovski, T. Austin, J. M. Lapetite, S. Ripplinger, and F. de Haan. 2016. "Recent Developments in Small Punch Testing: Tensile Properties and DBTT." *Theoretical and Applied Fracture Mechanics* 86:2–10. DOI: 10.1016/j.tafmec.2016.09.012.

[10] Altstadt, E., M. Houska, I. Simonovski, M. Bruchhausen, S. Holmström, and R. Lacalle. 2018. "On the Estimation of Ultimate Tensile Stress from Small Punch Testing." *International Journal of Mechanical Sciences* 136:85–93. DOI: 10.1016/j.ijmecsci.2017.12.016.

[11] Jackson, G. A., W. Sun, and D. G. McCartney. 2019. "The Influence of Microstructure on the Ductile to Brittle Transition and Fracture Behaviour of HVOF NiCoCrAlY Coatings Determined via Small Punch Tensile Testing." *Materials Science and Engineering A* 754:479–90. DOI: 10.1016/j.msea.2019.03.108.

[12] Bruchhausen, M., S. Holmström, J. M. Lapetite, and S. Ripplinger. 2017. "On the Determination of the Ductile to Brittle Transition Temperature from Small Punch Tests on Grade 91 Ferritic-Martensitic Steel." *International Journal of Pressure Vessels and Piping* 155:27–34. DOI: 10.1016/j.ijpvp.2017.06.008.

[13] Jeon, Jun Young, Yun Jae Kim, Sa Yong Lee, and Jin Weon Kim. 2016. "Extracting Ductile Fracture Toughness from Small Punch Test Data Using Numerical Modeling." *International Journal of Pressure Vessels and Piping* 139–140:204–19. DOI: 10.1016/j.ijpvp.2016.02.011.

[14] Xu, Yifei, and Kaishu Guan. 2013. “Evaluation of Fracture Toughness by Notched Small Punch Tests with Weibull Stress Method.” *Materials and Design* 51:605–11. DOI: 10.1016/j.matdes.2013.04.071.
[15] Dymáček, Petr. 2016. “Recent Developments in Small Punch Testing: Applications at Elevated Temperatures.” *Theoretical and Applied Fracture Mechanics* 86:25–33. DOI: 10.1016/j.tafmec.2016.09.013.
[16] Holmström, S., Y. Li, P. Dymacek, E. Vacchieri, S. P. Jeffs, R. J. Lancaster, D. Omacht, Z. Kubon, E. Anelli, J. Rantala, A. Tonti, S. Komazaki, Naveena, M. Bruchhausen, R. C. Hurst, P. Hähner, M. Richardson, and D. Andres. 2018. “Creep Strength and Minimum Strain Rate Estimation from Small Punch Creep Tests.” *Materials Science and Engineering A* 731:161–72. DOI: 10.1016/j.msea.2018.06.005.
[17] Lewis, D. T. S., R. J. Lancaster, S. P. Jeffs, H. W. Illsley, S. J. Davies, and G. J. Baxter. 2019. “Characterising the Fatigue Performance of Additive Materials Using the Small Punch Test.” *Materials Science and Engineering A* 754:719–27. DOI: 10.1016/j.msea.2019.03.115.
[18] CEN Workshop Agreement. 2006. “Small Punch Test Method for Metallic Materials.” *Small Punch Test Method for Metallic Materials*.
[19] Simonovski, Igor, Stefan Holmström, Daniele Baraldi, and Rémi Delville. 2020. “Investigation of Cracking in Small Punch Test for Semi-Brittle Materials.” *Theoretical and Applied Fracture Mechanics* 108:102646. DOI: 10.1016/j.tafmec.2020.102646.
[20] Campitelli, Emiliano N., P. Spätig, J. Bertsch, and C. Hellwig. 2005. “Assessment of Irradiation-Hardening on Eurofer97’ and Zircaloy 2 with Punch Tests and Finite-Element Modeling.” *Materials Science and Engineering A* 400–401(1-2 SUPPL.):386–92. DOI: 10.1016/j.msea.2005.02.088.
[21] Hill, Rodney. 1948. “A Theory of the Yielding and Plastic Flow of Anisotropic Metals.” *Proceedings of the Royal Society of London. Series A. Mathematical and Physical Sciences* 193(1033):281–97. DOI: 10.1098/rspa.1948.0045.
[22] Okuda, Naoyuki, Ryuta Kasada, and Akihiko Kimura. 2009. “Statistical Evaluation of Anisotropic Fracture Behavior of ODS Ferritic Steels by Using Small Punch Tests.” *Journal of Nuclear Materials* 386–388(C):974–78. DOI: 10.1016/j.jnucmat.2008.12.265.
[23] Ma, Young Wha, and Kee Bong Yoon. 2010. “Assessment of Tensile Strength Using Small Punch Test for Transversely Isotropic Aluminum 2024 Alloy Produced by Equal Channel Angular Pressing.” *Materials Science and Engineering A* 527(16–17):3630–38. DOI: 10.1016/j.msea.2010.02.057.
[24] Turba, K., R. C. Hurst, and P. Hähner. 2012. “Anisotropic Mechanical Properties of the MA956 ODS Steel Characterized by the Small Punch Testing Technique.” Pp. 76–81 in *Journal of Nuclear Materials*. Vol. 428. DOI: 10.1016/j.jnucmat.2011.08.042.
[25] Moreno-Valle, E. C., W. Pachla, M. Kulczyk, B. Savoini, M. A. Monge, C. Ballesteros, and I. Sabirov. 2013. “Anisotropy of Uni-Axial and Bi-Axial Deformation Behavior of Pure Titanium after Hydrostatic Extrusion.” *Materials Science and Engineering A* 588:7–13. DOI: 10.1016/j.msea.2013.08.044.
[26] Serrano, M., A. García-Junceda, R. Hernández, and M. H. Mayoral. 2014. “On Anisotropy of Ferritic ODS Alloys.” *Energy Materials: Materials Science and Engineering for Energy Systems* 9(3):1664–68. DOI: 10.1179/1743284714Y.0000000552.
[27] Altstadt, E., M. Serrano, M. Houska, and A. García-Junceda. 2016. “Effect of Anisotropic Microstructure of a 12Cr-ODS Steel on the Fracture Behaviour in the Small Punch Test.” *Materials Science and Engineering A*. DOI: 10.1016/j.msea.2015.12.055.
[28] Altstadt, E., F. Bergner, A. Das, and M. Houska. 2019. “Effect of Anisotropic Microstructure of ODS Steels on Small Punch Test Results.” *Theoretical and Applied Fracture Mechanics* 100:191–99. DOI: 10.1016/j.tafmec.2019.01.014.
[29] Song, Ming, Kaishu Guan, Wen Qin, and Jerzy A. Szpunar. 2012. “Comparison of Mechanical Properties in Conventional and Small Punch Tests of Fractured Anisotropic A350 Alloy Forging Flange.” *Nuclear Engineering and Design* 247:58–65. DOI: 10.1016/j.nucengdes.2012.03.023.
[30] Kulkarni, R. V., K. V. Mani Krishna, S. Neogy, D. Srivastava, E. Ramadasan, G. K. Dey, N. Saibaba, S. K. Jha, R. S. Shriwastaw, and S. Anantharaman. 2013. “Determination of Correlation Parameters for Evaluation of Mechanical Properties by Small Punch Test and Automated Ball Indentation Test for Zr-2.5% Nb Pressure Tube Material.” *Nuclear Engineering and Design* 265:1101–12. DOI: 10.1016/j.nucengdes.2013.10.009.
[31] Rezaei, Ali, Ahmad Rezaeian, Ahmad Kermanpur, Mohsen Badrossamay, Ehsan Foroozmehr, Mahdi Marashi, Ali Foroozmehr, and Jeongho Han. 2020. “Microstructural and Mechanical Anisotropy of Selective Laser Melted IN718 Superalloy at Room and High Temperatures Using Small Punch Test.” *Materials Characterization* 162:110200. DOI: 10.1016/j.matchar.2020.110200.
[32] Bruchhausen, M., E. Altstadt, T. Austin, P. Dymacek, S. Holmström, S. Jeffs, R. Lacalle, R. Lancaster, K.

Matocha, and J. Petzova. 2018. “European Standard on Small Punch Testing of Metallic Materials.” *Ubiquity Proceedings* 1(S1):11. DOI: 10.5334/uproc.11.

[33] Okada, A., M. L. Hamilton, and F. A. Garner. 1991. “Microbulge Testing Applied to Neutron Irradiated Materials.” *Journal of Nuclear Materials* 179–181(PART 1):445–48. DOI: 10.1016/0022-3115(91)90120-V.

[34] Calaf-Chica, Jose, Pedro Miguel Bravo Díez, Mónica Preciado Calzada, and Maria Jose Garcia-Tarrago. 2020. “Optimization of the t/10 Offset Correlation Method to Obtain the Yield Strength with the Small Punch Test.” *Journal of Nuclear Materials* 534:152177. DOI: 10.1016/j.jnucmat.2020.152177.

[35] Calaf-Chica, Jose, Pedro Miguel Bravo Díez, Mónica Preciado Calzada, and Daniel Ballorca-Juez. 2019. “A Systematic FEM Analysis of the Influence of Mechanical Properties in the Reliability of the Correlation Methods in the Small Punch Test.” *International Journal of Mechanical Sciences* 153–154:299–309. DOI: 10.1016/j.ijmecsci.2019.02.013.